DDSim: Framework for Multiscale Structural Prognosis

by
John Emery, Ph.D.
Solid Mechanics Division
Sandia National Laboratories
Albuquerque, NM 87113
505-844-3411
jmemery@sandia.gov

Anthony R. Ingraffea
Dwight C. Baum Professor of Engineering
Cornell Fracture Group
643 Rhodes Hall
Cornell University
Ithaca, NY 14853 USA
607-341-0043
ari1@cornell.edu

1 PROLOGUE: 2025

On June 1, 2025, Boeing delivers the first B-17 HyperFortress, tail number 20-0001, a Mach 6 aircraft. Along with this physical instantiation of the aircraft, Boeing also delivers an as-built *digital instantiation* of this tail number, 20-0001D/I. 20-0001D/I is a 1000 billion DOF, hierarchical, computational structures model of 20-0001. This "Digital Fortress" is ultra-realistic in geometric detail, including manufacturing anomalies, and in material detail, including the statistical microstructure level. 20-0001D/I accepts probabilistic input of loads, environmental, and usage factors, and it also tightly couples to an outer-mold-line, as-built, CFD model of 20-0001.

20-0001D/I can be virtually flown over a 1 hour, design-point flight in 1 hour on an exaflop-scale high-performance computer. During each such virtual flight, 20-0001D/I accumulates usage damage according to best-physics-based, probabilistic simulations, and outputs about 1 petabyte of material, structural performance, and damage data. 20-0001D/I is "flown" for 1000 hours during ground testing of 20-0001. During this accelerated, preliminary lifing, a number of unexpected limit states are encountered leading to loss of primary structural elements, with 2 incidents likely leading to loss of aircraft forecast. Appropriate repairs, redesigns, and retrofits are planned and implemented on 20-0001 before its first flight to preclude such events from actually occurring. The HyperFortress becomes the first Air Force flight vehicle to be certified mostly through simulation.

It is recognized, however, that design-point usage is always trumped by actual usage, involving unplanned mission types and payloads. Therefore, a second digital instantiation, 20-0001D/A, is linked to the structural

sensing system deployed on 20-0001. This structural health monitoring system records, at high frequency, actual, six-DOF accelerations, as well as surface temperature/pressure readings during each actual flight of 20-0001. Each hour of real flight produces about 1 petabyte of such real data. These data are input into the 20-0001D/A structural model, and this model itself becomes a virtual sensor, interpolating sparse acquired data over the entire airframe. Using Bayesian statistical techniques, 20-0001D/I is periodically updated to reflect actual usage recorded by 20-0001 and by 20-0001D/A, and is rerun for prognosing the remaining life of 20-0001, and for updating reliability estimates for all primary structural components. This prognosis leads to time-and-budget-appropriate execution of rehab plans resulting from such updated lifing and reliability estimates. This process is being executed for all 12 of the HyperFortress aircraft.

2 INTRODUCTION

From the perspective of the air forces of the U. S. military, the capabilities envisioned in the prologue to this chapter are what this book is all about. What science and technology, what simulation systems, need to be discovered and developed to make this vision possible? Can complex structural airframe and engine systems, to be operated in ever more extreme conditions, be designed and certified mostly though computer simulation? Can tail-number-specific, reliability-informed, condition-based maintenance replace fleet-wide damage tolerance procedures with their attendant high inspection costs? To answer “yes” to these questions does not require a fundamentally new approach to thinking about how to design, build, and maintain predictably safe structures: make sure driving

"forces" determined from response analyses are always acceptably less than resisting "forces" defined through test and theory, lest one exceed a structural limit state. *Rather, what is required is confidence in the belief that one can replace most of the testing needed to uncover and quantify material and structural limit states with reliability predictions based on understanding of the rules of physics and mechanics, expressed in computer code, and executed on our most advantageous tool—nearly infinite computing power.*

A graphical depiction of the hierarchical computational simulation system of a "digital aircraft" is shown in Figure 1. The OEM would deliver as-built geometry and numerical models of each primary structural component, Figure 1a. These models can be analyzed at any time during acceptance trials or during actual aircraft life to determine current field responses. These analyses would flag "hot spots", likely to lead to a local limit state, such as fatigue crack initiation, Figure 1b. At each such indication, a lower length-scale model is introduced, involving all the microstructural modeling, constitutive behavior, and damage modes discussed in earlier chapters of this book, Figure 1c. Multiscaling techniques, also addressed in this book, inform these models of evolving fields at the structural scale, Figure 1d, and damage evolution is simulated at the microstructural scale, Figure 1e. Information concerning stiffness and strength changes resulting from such evolution is periodically up-linked to the structural scale model, and its remaining life and residual strength are probabilistically estimated, Figure 1f.

The purpose of this chapter is to describe a prototype hierarchical computational simulation system, a Damage and Durability Simulator (DDSim), as it would apply to prognosis of fatigue life of a major airframe component. In the next section, the architecture of DDSim is described.

Each level of its hierarchy is described in following sections, and these are interconnected with the thread of a consistent example problem. In each section, the relevance of a DDSim-like environment to the vision in the prologues is highlighted, and the major shortcomings in our present capabilities to reach this vision are identified.

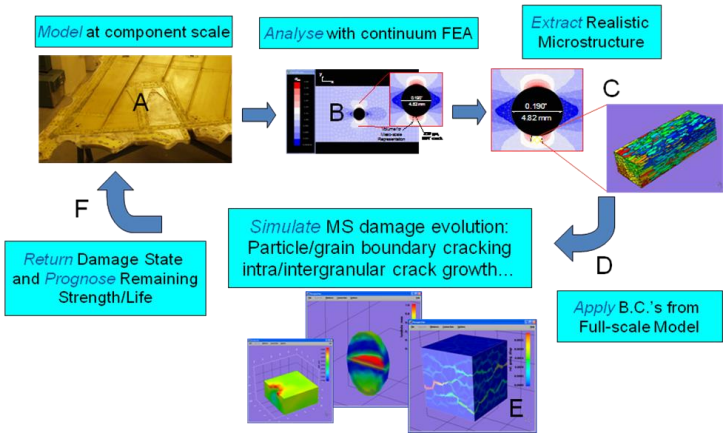

Fig. 1. Graphical depiction of information flow in the hierarchical computational simulation system of the "digital aircraft" of the future. Probabilistic prognosis of fatigue life instanced here.

3 DDSIM ARCHITECTURE

Those 1000 billion degrees-of-freedom (DOF) and petabyte databases associated with the "Digital Fortress" have to be hierarchical and tightly integrated. Many computational models, at different length/time scales, and with multi-physics coupling will consume those DOF over an entire air vehicle. Data associated with response analyses from these models needs to be mined for indications of impending problems, and health prognoses will then need to be performed by projecting damage evolution forward with even more computational models. DDSim is a rudimentary

prototype of a system that embodies these needs in the context of fatigue cracking.

DDSim, employs an hierarchical "search and simulate" strategy consisting of three main levels. The strategy assumes that the total fatigue life of a structure can be decomposed as

$$N^T = N^{MLC} \oplus^{a^{MLC}} N^{MSC} \qquad (*.1)$$

where N^T is the total fatigue life of the structure, N^{MLC} is the number of loading cycles consumed by microstructurally large crack (MLC) growth processes, N^{MSC} is the number of loading cycles consumed by microstructurally small crack (MSC) growth processes, and a^{MLC} is the characteristic length of a crack when it can be considered microstructurally large.

The operator $\oplus^{a^{MLC}}$ implies summation that is dependent on the definition of a^{MLC} which can be arbitrarily chosen by the engineer. The notation here will use capital letters to denote random variables and lower case letters to represent deterministic variables or specific samples of a random variable. Hence, while N^T is the random variable representing total fatigue life of the structure described by a probabilistic distribution, n^T is one realization of that total life and is given by an integer value of cycles.

For a structural component subject to a given loading program, the functional dependence of N^T can be expressed by

$$N^T = N^T(\boldsymbol{X}, \boldsymbol{A}, \boldsymbol{E}) \qquad (*.2)$$

where $\boldsymbol{X} \in \mathcal{R}^3$ is the dominant flaw location, $\boldsymbol{A} \in \mathcal{R}^p$ is a p-dimensional array describing flaw geometry and $\boldsymbol{E} \in \mathcal{R}^s$ is a s-dimensional array describing material resistance to crack growth. Because N^T is a function of the random vectors $\boldsymbol{X}$, $\boldsymbol{A}$ and $\boldsymbol{E}$, N^T is a random variable. Consequently, the

total fatigue life of a structural component has the cumulative distribution function (CDF)

$$F_{N^T}(n^T) = P\left[N^T(\boldsymbol{X},\boldsymbol{A},\boldsymbol{E}) \le n^T\right] \qquad (*.3)$$

where N^T is the random variable and n^T represents its possible values. Furthermore, the probability of failure at a specified critical number of cycles is defined as

$$P_f = P\left[N^T(\boldsymbol{X},\boldsymbol{A},\boldsymbol{E}) \le n_{cr}^T\right] = F_{N^T}(n_{cr}^T) \qquad (*.4)$$

where n^T_{cr} is the critical number of loading cycles. The reliability of the structure is the probability of non-failure and can be readily computed as

$$P\left[N^T(\boldsymbol{X},\boldsymbol{A},\boldsymbol{E}) > n_{cr}^T\right] = 1.0 - P_f \qquad (*.5)$$

A flowchart showing the architecture of DDSim is shown in Figure 2. The components in the flowchart bear the following significance:

- Dashed boxes indicate user input/control into the system;
- Solid rectangular boxes indicate operations within the system (bold for primary hierarchical components);
- Diamonds indicate decision points;
- Ovals indicate probabilistic life predictions (output); and
- Arrows indicate the direction of data flow.

The components above the dashed line are collectively labeled the "predictor". Shown as input to the predictor are the, generally, stochastic data supporting the simulation.

Level I operates on this data and the output is a low fidelity estimate of the probability of failure. Then, the first diamond in the data flow asks if refined fidelity is necessary and passes data along or exits, accordingly. If refinement is necessary, the low fidelity estimate becomes the prediction of reliability to be corrected by subsequent analyses, and the data enters the "corrector", actions below the dashed line. The first step in the

corrector requires intelligent control to select hot-spots. The corrector improves fidelity by operating on a subregion of the original domain. The volume of this subdomain is appropriately chosen surrounding a hot-spot. Recalling equation *.1, there are obvious ways to improve the Level I prediction of reliability: improve the estimate of N^{MLC}, and/ or improve the estimate of N^{MSC}. DDSim Levels II and III address these opportunities.

Level II operates at the selected hot-spots to improve the estimate of N^{MLC} which can be combined through equation *.1 to provide an improved estimate of the total structure reliability. Upon exiting Level II, the level of

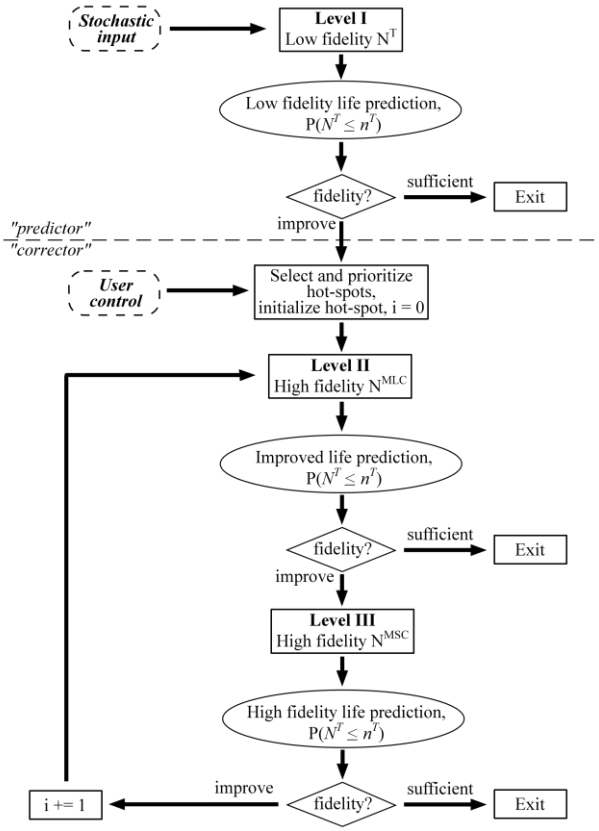

Fig. 2. Flowchart showing the 3-level architecture of DDSim.

fidelity is again assessed and the decision to continue refinement or exit is made.

If continued refinement is necessary, Level III operates at the selected hot-spots to improve the estimate of N^{MSC}. The Level III tool is generally the most computationally expensive, as it is the bridge between length scales. Consequently, Level III requires intelligent control to determine size and number of microstructural simulations. The final result of the simulation will be a higher fidelity structural reliability estimate than that obtained using only Level I. If the fidelity of this reliability estimate is insufficient, the engineer must refine the model. Obviously, there are three ways to control the quality of the final estimate of reliability. First, one could provide higher resolution input data and run the entire system again. Second, one could include a larger subset of the original domain to be analyzed in the corrector by selecting additional hot-spots. Finally, one could include more or larger microstructural simulations. It should be emphasized that the decomposition indicated in Equation *.1 is not intended to suggest that N^T is evenly divided in two parts. In fact, N^{MSC} can consume most of N^T. If that is the case, it may not be cost effective to use Level II, and one can choose to skip directly to Level III. Conversely, for a vehicle already in service, the average microstructurally large crack length may be known by NDE. If so, the Level III simulation might be too costly and unnecessary, and one could stop the simulation after Level II.

In the following sections, each of these levels is described and its usage is exemplified through a consistent, simple example problem, the stiffened wing panel shown in Figure 3. Proprietary physical testing on this example has been performed (Papazian et al. 2007a; 2007b). Although specific geometrical data associated with this component cannot be

presented here, results from this testing will help to identify the validity and shortcomings of reliability predictions based on current capabilities.

Space limitations here preclude detailed descriptions of all the functions of DDSim, all levels; the reader can refer to Emery (2007) and Emery et al. (2008) for more details.

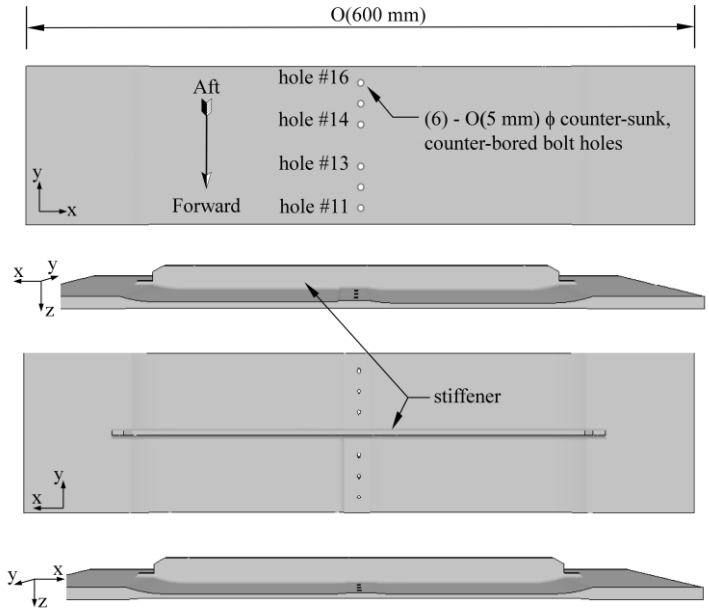

Fig. 3. Example application problem for 3 levels of DDSim. Stiffened wing panel is loaded in tension in the x-direction.

4 DDSIM LEVEL I: REDUCED-ORDER, PROBABILISTIC, LOW-FIDELITY LIFE PREDICTION AND INITIAL SCREENING

Essentially, Level I in DDSim is an automated way of performing state-of-practice, damage tolerance type assessments at every possible flaw location in a structure, Figure 4. DDSim Level I is a generalization and

automation of the approach taken in such familiar codes as NASGRO [2008] or AFGROW [2008]. Level I idealizes the initial crack geometry as penny-shaped, semi-circular, or quarter-circular, and uses analytically computed stress intensity factor (SIF) versus crack size solutions to compute crack driving forces. These solutions are then related to crack growth rate through standard relationships, and these are integrated to predict crack size versus number of cycles. The result is a low fidelity reliability estimate that can be used for preliminary design, selection of subdomains to perform the higher level simulations, and as the prediction to be corrected by the higher order analyses of Levels II and III. Level I produces a highly automated, probabilistic, conservative, and fast prediction of fatigue life.

Inputs to Level I are distributions of initial crack radii, a finite element (FE) mesh and boundary conditions for the component, the finite-element-generated stress analysis results, and required material parameters for the requested crack growth rate model. The user-defined initial crack sizes can be described deterministically, randomly by distribution, or randomly through the use of a particle cracking filter for materials where intrinsic flaw size is correlated with second phase particle size. For the example component described herein, this last option uses a particle cracking filter described by Bozek et al. (2008) specific to AA 7075-T651, the material used in the component shown in Figure 3.

The input FE model can be of arbitrary geometrical complexity, and many such models would be expected to represent the possibly hundreds of primary structural components in a digital aircraft. This FE model does not include damage; rather, it represents structure-scale behavior using standard continuum behavior models. The results from the stress analysis

are input as nodal stresses, but could be any other field variable specific to the component and its material systems.

For a deterministic analysis, Level I uses the nodal stresses in conjunction with the initial crack size and analytically computed SIF solutions to compute SIFs for the assumed crack at each FE node. The orientation of the initial crack is assumed to be perpendicular to the local maximum principal tensile stress at the node, and no crack interaction is

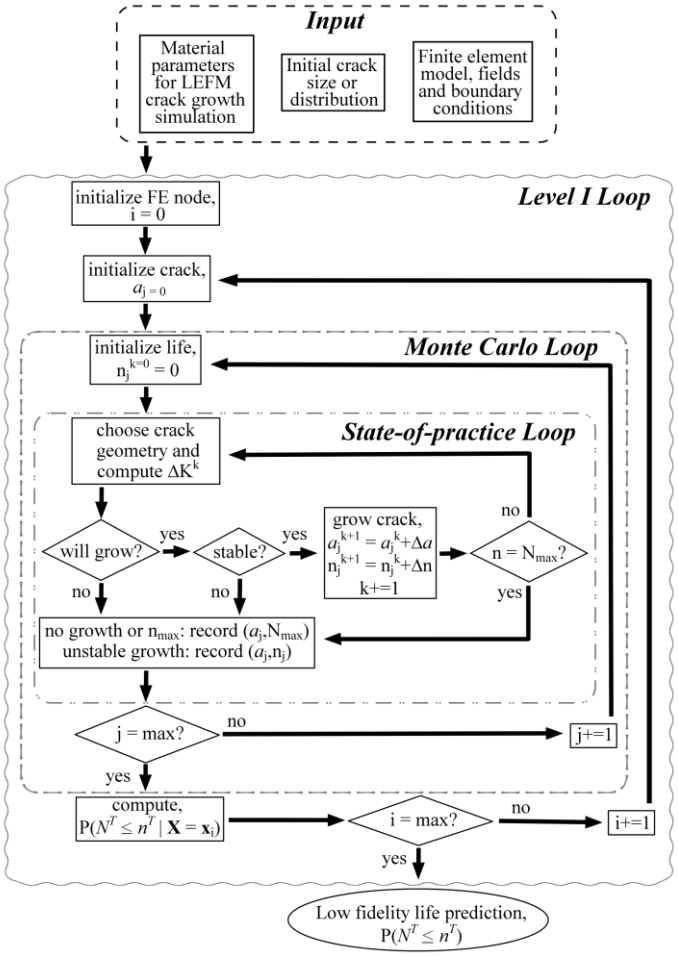

Fig. 4. Flowchart of DDSim Level I operations.

currently allowed. The use of analytically computed SIF solutions is the main source of speed, and subsequently, reduced order accuracy. Level I combines the SIFs with input material parameters and empirical models to calculate the crack growth rate. With the growth rate, a new crack size is computed and the procedure is repeated for each load cycle. Following this procedure, Level I performs an automated interrogation resulting in a life prediction at every FE node. This produces a deterministic scalar field of life prediction computed over the entire domain of the component.

For probabilistic life assessment, Level I performs Monte Carlo simulation using the procedure outlined above for each initial crack radius from its distribution. Assuming the initial crack radii are less then a^{MLC}, the result at one node is a list of life predictions that corresponds to the list of initial crack sizes, or

$$\boldsymbol{n}_I^T = \{n_1^T, n_2^T, \ldots, n_l^T\} \qquad (*.6)$$

where the subscript *I* indicates that this is the Level I estimate, the n_j^T are the number of load cycles computed corresponding to initial crack size j, and l is the total number of initial crack sizes. $\boldsymbol{n}_I^T$ represents a list of samples from the conditional distribution of total fatigue life given the event that a crack originates at node i,

$$F_{N^T|\boldsymbol{x}}(n^T) = P\left[N^T(\boldsymbol{X}, A) \le n^T \mid \boldsymbol{X} = \boldsymbol{x}_i\right] \qquad (*.7)$$

where $\boldsymbol{A} \in \mathcal{R}$ is the random initial crack radius, and $\boldsymbol{x}_i \in \mathcal{R}^3$ is the position of node i. The conditional probabilities for each node are combined, via the theorem of total probability, to give the cumulative probability of failure of the component as

$$F_{N^T}(n^T) = \sum_{i=1}^{m} P\left[N^T(\boldsymbol{X}, A) \le n^T \mid \boldsymbol{X} = \boldsymbol{x}_i\right] \cdot P(\boldsymbol{X} = \boldsymbol{x}_i) \qquad (*.8)$$

where m is the total number of nodes in the FE model, and $P(\boldsymbol{X} = \boldsymbol{x}_i)$ is the probability that the flaw originates at node i. The distribution for flaw origination is assumed to be uniform or, in the case of Bozek's particle cracking criteria (2008), explicitly given by the ratio between the number of broken particles at a damage origin divided by the total number of broken particles. Finally, the probability of failure at some critical number of load cycles, n^T_{cr}, is

$$P_f = F_{N^T}(n^T_{cr}) = P\left[N^T(\boldsymbol{X}, A) \le n^T_{cr}\right] \qquad (*.9)$$

and the reliability, R, is computed as the probability of non-failure,

$$R = P\left[N^T(\boldsymbol{X}, A) > n^T_{cr}\right] = 1.0 - P_f \qquad (*.10)$$

where n^T_{cr} is some critical life measure.

Since the Level I simulation involves l life predictions at m FE nodes, there are $l \times$ m fatigue life predictions required. For reasonable FE meshes with a reasonable sample of initial crack radii, the number of fatigue life predictions can readily climb into the millions. This can be reduced, for example, by only considering surface nodes. However, with the parallel processing capability currently implemented in DDSim, large simulations can be completed in relatively short amounts of time. For the example considered here, DDSim Level processed 10,000 initial flaw sizes at about 64,000 surface nodes, in about 15 minutes on 340 processors (single core, 3.6 GHz, about 10^{12} FLOPS). For the "Digital Fortress", parallel, exascale (10^{18} FLOPS, about 10,000 multi-core processors, about a billion times faster than current desktop computers) computers would make very short work of a Level I filter on all its primary structural components.

Since the result of the Level I simulation is a scalar field, the conditional probability, or mean life prediction, or any other meaningful statistic, can be easily color-contoured and plotted on the surface of a

component for effective visualization of results, as will be shown below in the example problem. This facilitates post-processing and provides visual guide to regions that are particularly susceptible to fatigue damage. No doubt an immersive stereo visualization of the "Digital Fortress", with all its hot spots color coded for priority, would be available at maintenance depots.

Finally, the hot-spot locations are selected from the FE node locations using a criterion based on the Level I life prediction. Three criteria easily identified are: conditional probability of failure, absolute lowest life, and mean life. In this chapter, the minimum mean life prediction is used on the example component. The resulting hot-spot is the one FE node location which has the lowest average Level I life prediction.

4.1 Application of DDSim Level I to Example Problem

Figure 3 shows the geometry of the example problem. DDSim Level I was applied to this problem under constant amplitude and spectrum loading conditions. The component has six countersunk, counter-bored bolt holes at mid-length which cause large, but differing, stress concentrations. The component was machined from rolled AA 7075-T651 plate. The specimen is modeled such that the x-direction corresponds to the material rolling direction (RD), the y-axis corresponds to the transverse direction (TD) and the z-axis corresponds with the normal direction (ND). This geometry is purposely *not symmetric* about the stiffener. There are two sources of asymmetry. First, the component is thicker for holes #11-13 than for holes #14-16. Second, the space between hole 16 and the aft edge of the specimen is less than the space between hole 11 and the forward edge of the specimen.

Figure 5a shows the surface FE mesh on the model and 5b a close-up at one of the bolt holes. There were 140,024 8-noded brick elements and 184 6-noded wedge elements in the input to DDSim. There are 63,974 nodes on the surface of the model.

Figure 6 shows the boundary conditions used in the model. The applied load for the spectrum loading corresponds to the maximum load in the spectrum. This spectrum, which contains many over- and underload excursions, was developed at the Northrop Grumman Corporation (NGC) to model the service loads experienced by military aircraft. The applied load for the constant amplitude simulation corresponds to the root mean square (RMS) of the spectrum. The maximum load in the spectrum was 316.8 kN. In the constant amplitude loading analysis, the RMS load, 177.9 kN, was applied with R = 0. The constitutive model was linear elastic, isotropic.

Crack growth rate was computed using the familiar NASGRO equation (Forman and Mettu 1992). The material properties used with this equation were taken from the NASGRO (2008) material database for AA 7075-T651.

The distribution of a set of 10,000 potential flaw radii is shown in Figure 7. This distribution was then passed through the filter developed by Bozek et al. (2008) to produce a subset of final flaw radii, a function of the state (stress, grain orientation, etc.) at each node location.

Figure 8 shows the mean life prediction contour plot for the component under the spectrum loading program with initial flaw sizes from the particle cracking filter. The lowest mean life prediction is 29,058 cycles, which occurs at the aft side of hole 16, near the intersection of the counter-bore with the main-bore. Figure 9 shows the predicted reliability of the

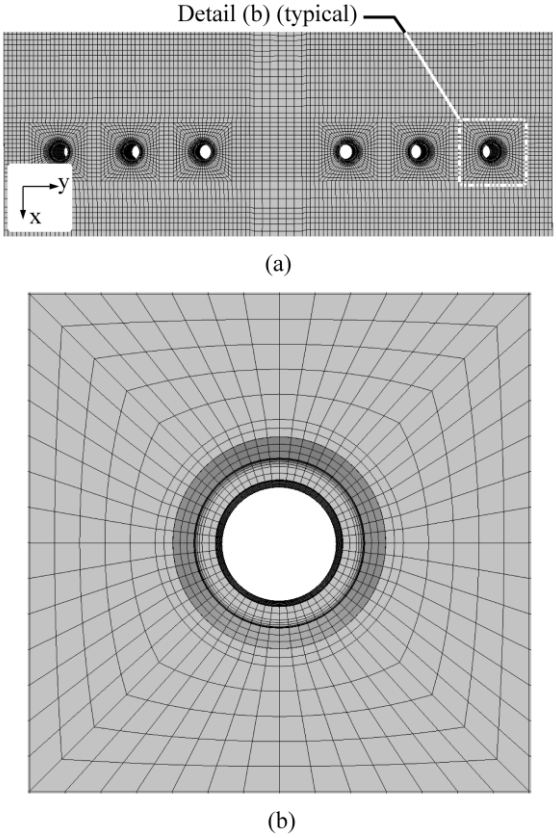

Fig. 5. Finite element model of example problem. (a) Surface mesh on unstiffened side. (b) Typical detail around fastener hole.

component. This figure includes the results from the constant amplitude and spectrum loading programs.

The fatigue surfaces in hole 16 showed large crack growth increments towards the outward edge of the fatigue fatigue crack in the aft side of hole 16 had the largest growth increments and the greatest surface area and, therefore, appeared to be the dominant crack. From these surfaces, it is evident that the origin of the fatigue cracks, in particular the dominant

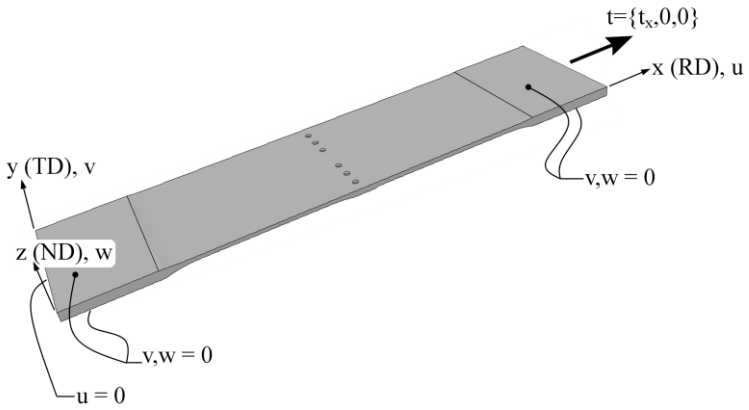

Fig. 6. Boundary conditions applied to FE model of example problem.

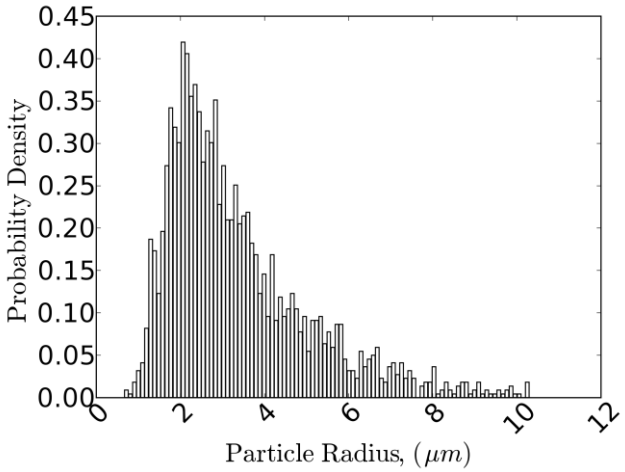

Fig 7. Distribution of potential flaw size used in the particle cracking filter (Bozek et al. 2008) for DDSim Level I.

crack, is near the corner created by the intersection of the counter-bore with the main-bore. The Level I simulation matches this observation.

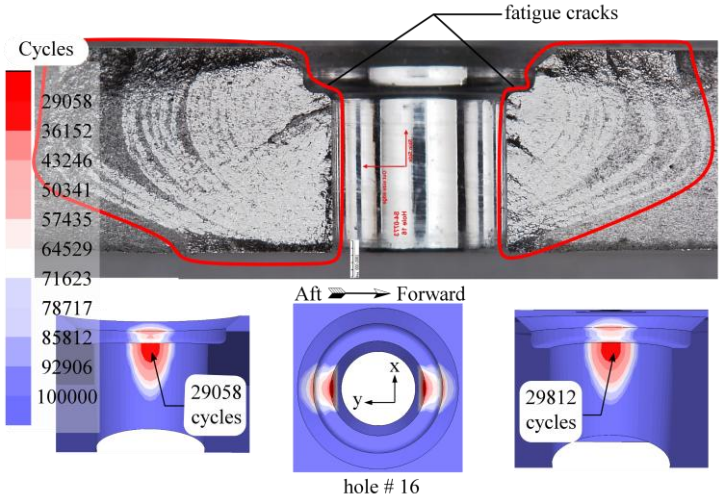

Fig. 8. Above, fracture surface at hole 16 in actual component, showing origins of fatigue cracks at shoulder of counterbore. Below, Level I prediction of location of minimum life flaw, and the average life prediction for the example problem under variable amplitude loading with 10,000 initial particles.

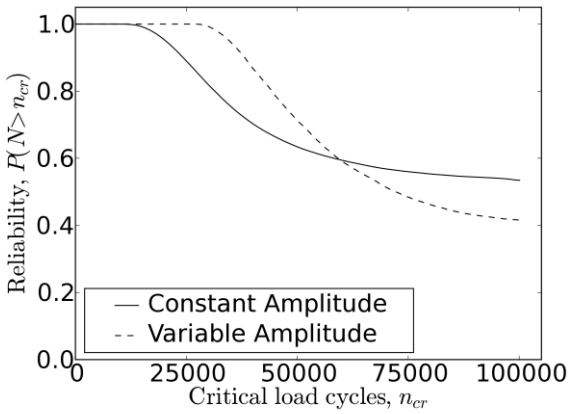

Fig 9. Reliability prediction for the example component under both constant amplitude and variable amplitude loading with initial flaws generated with the particle cracking filter.

5 DDSIM LEVEL II: HIGH-FIDELITY, MICROSTRUCTURALLY LARGE CRACK GROWTH SIMULATION

DDSim Level II is the second tier in the hierarchical fatigue life simulation. Level II performs high fidelity computations for the number of cycles consumed by microstructurally large crack growth, n^{MLC}. The primary technical advances offered by Level II are automated crack insertion at hot-spot locations determined from the Level I results, and support for cracks or arbitrary shape and orientation in a component of complex geometry and boundary conditions. The hot-spot selection is based on the mean Level I life prediction. The three-dimensional crack growth simulations are conducted with the fracture analysis code FRANC3D/NG (2008). FRANC3D/NG performs its fracture mechanics computations based on field data obtained through any suitable FE analysis code.

Carter et al. (2000) describe crack growth simulation as an incremental process, where a series of steps are repeated for a progression of models. Each increment of the simulation relies on previously computed results and represents one crack configuration. There are four primary databases required for each increment. The first is the representational database, denoted by $\boldsymbol{R}_i$, where the subscript identifies the increment number. The representational database contains a description of the solid model geometry, including the cracks, the boundary conditions and the material properties. The representational database is transformed by a discretization process $\boldsymbol{D}$ to a stress analysis database $\boldsymbol{\Sigma}_i$. The discretization process includes a meshing function $\boldsymbol{M}$:

$$\boldsymbol{D}(\boldsymbol{R}_i, \boldsymbol{M}(\boldsymbol{R}_i)) \Rightarrow \boldsymbol{\Sigma}_i \qquad (*.11)$$

Level II automatically modifies the structural scale FE model from Level I to include the microstructurally large crack with characteristic dimension a^{MLC}. The automatic crack insertion orients the crack perpendicular to the local maximum principal stress direction. The uncracked FE model that was read into Level I as input is first converted to the representational database. Then, the database is altered to account for the new geometry of the crack surface. At this point, the original discritization is no longer valid because the background geometry has changed. Hence, a new mesh must be created using the discretization process $\boldsymbol{D}$. The meshing function in DDSim uses an advancing front algorithm that originated with the work of Neto et al. (2001, 2008). FRANC3D/NG (2008) surrounds the crack front with a template of well-formed, singular, crack-front elements.

The analysis database contains a complete, but approximate, description of the body suitable for input to a solution procedure, $\boldsymbol{S}$, often a finite or boundary element stress analysis program. Any suitable analysis program is sufficient; however, in the example problem in this chapter the commercial FE code, ANSYS (2008), was used. The analysis database, $\boldsymbol{\Sigma}_i$, is exported to the analysis program where the solution procedure, $\boldsymbol{S}$, is used to transform $\boldsymbol{\Sigma}_i$ to an equilibrium database, $\boldsymbol{Q}_i$. The equilibrium database consists of field variables, such as displacements and stresses that define the equilibrium solution and contains appropriate material state information:

$$\boldsymbol{S}(\boldsymbol{\Sigma}_i) \Rightarrow \boldsymbol{Q}_i \qquad (*.12)$$

The equilibrium database is then read back into FRANC3D/NG where it is converted to the crack driving forces database, $\boldsymbol{K_i}$, with the fracture mechanics procedure, $\boldsymbol{F}$:

$$\boldsymbol{F(Q_i)} \Rightarrow \boldsymbol{K_i} \qquad (*.13)$$

Mixed-mode SIF's are automatically computed in FRANC3D/NG using the M-integral approach, Banks-Sills et al. (2005, 2007). By means of an update function, $\boldsymbol{U}$, $\boldsymbol{K_i}$, in conjunction with $\boldsymbol{R_i}$, is used to create a new representational model $\boldsymbol{R_{i+1}}$, which includes the crack growth increment. The crack growth function, $\boldsymbol{C}$, which is part of $\boldsymbol{U}$, determines the shape and extent of the crack growth increment:

$$\boldsymbol{U(R_i, C(K_i))} \Rightarrow \boldsymbol{R_{i+1}} \qquad (*.14)$$

This sequence of operations is repeated until a suitable termination condition is reached. The flowchart presented in Figure 10 illustrates the path of data flow in the context of the Level II simulation. Of course, other approaches for simulating growth of cracks in a computational model are available. The advantages and disadvantages of these are discussed in Ingraffea (2008).

The representation, analysis, and equilibrium databases would consume much of the petabytes of data used in tracking the life of the "Digital Fortress". Results of such a simulation might include one or more of the following: a final crack geometry, a loading versus crack size history, a crack opening profile or a history of the crack-front fracture parameters. When a suitable stopping criterion is met, the SIF history is integrated to produce an estimate for the number of cycles consumed by microstructurally large crack growth. Following the integration, the Level I life prediction is updated. The following section elaborates on these processes.

5.1 Input and the FRANC3D/NG Loop

The input required for a Level II analysis is the following:

- Level I life prediction;
- A hot-spot location and crack orientation; and
- The complete structural scale FE model.

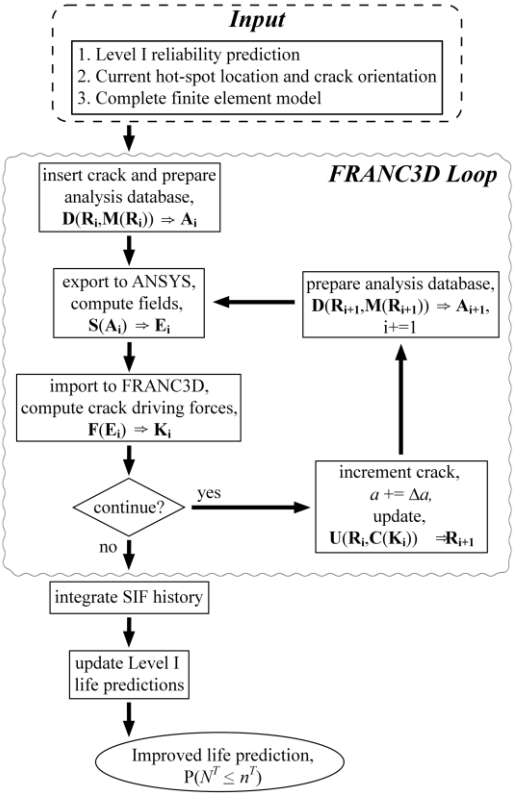

Fig. 10. Flowchart of DDSim Level II operations.

Level II uses the complete, structural scale FE model to create its representational database. This does not require any additional user effort because the entire model, including boundary conditions, was input to Level I. In the case of variable amplitude loading, the analysis database is

computed for a single loading with the assumption that linear superposition is valid. The choice is arbitrary and user defined, but in the example shown herein the maximum load in the spectrum was used. During the SIF history integration phase, the driving force is scaled appropriately to correspond with the load at the current cycle in the spectrum.

The output from the FRANC3D/NG is the history of the crack driving force database $\{\boldsymbol{K_0}, ..., \boldsymbol{K_n}\}$, where the subscript n is the total number of increments in the loop. This history relates crack length to the corresponding SIF. The integration routine treats discrete points along the crack front as separate, non-interacting cracks in a two-dimensional body.

Crack *length* is ill-defined for a crack in a three-dimensional body because a crack is actually a two-dimensional manifold, so a convenient convention is adopted. The crack length for Level II is defined as the distance along the set of straight-lines connecting a discrete crack front point. The crack front point is given by the normalized crack front position. The dash-dot line in Figure 11 illustrates the crack length for the mid-point, B_i, along a crack front. This illustration is for a very large crack increment; smaller increments generally lead to a more accurate representation.

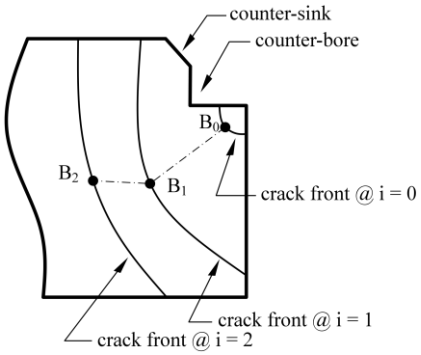

Fig 11. The crack length for point B_i at crack increment i = 0, 1, 2.

The SIF history is extracted from the $\{\boldsymbol{K_0}, ..., \boldsymbol{K_n}\}$ database with a utility which requires the normalized crack front point to be specified. The integration routine uses a modified version of the state-of-practice loop from Level I. However, in place of the analytical SIF solutions used in Level I, the FE-computed SIF history is interpolated to compute the cyclic crack driving force. The integration is conducted at each crack front point considered, and the minimum is taken as the high-fidelity estimate of the number of cycles consumed by microstructurally large crack growth, N^{MLC}. In the example in this chapter, three crack front points are used. One point is used at each surface-breaking location and one is used at the mid-point of the crack front. The final step in the Level II process is to update the prediction from Level I.

5.2 Application of DDSim Level II to Example Problem

In this section, one hot-spot in the example component is evaluated with DDSim Level II. A crack is inserted at the hot-spot with the lowest mean life prediction computed in the Level I simulation under variable amplitude loading with the initial flaws determined by the particle cracking filter.

The lowest mean total life prediction from that data set was 29,058 cycles with a crack originating from the intersection between the counter-bore and main-bore at the aft side of bolt hole 16. The Level II result should be an improvement of the Level I fatigue life estimate. The following subsections describe the cracked model, the updated Level I prediction and discussion.

To facilitate the crack insertion process, a subregion of the structural-scale mesh was used to prepare the initial analysis database, Σ_o, around bolt hole 16. Figure 12 (a) shows a portion of this subregion at the aft edge of bolt hole 16 and the surface mesh. Figure 12(b) is a cross-section in the plane of the aft edge crack showing the quarter-penny shaped initial crack of size a^{MLC} = 0.381 mm, the default initial crack size for MLC.

There were a total of 13 crack increments used in the Level II simulation, Figure 13. Although the predicted cracks could have taken any shape, unrestricted by the mesh model, they remained essentially in their original plane, perpendicular to the local maximum principal stress direction at the crack origin. Figure 13 shows the fracture surface of the

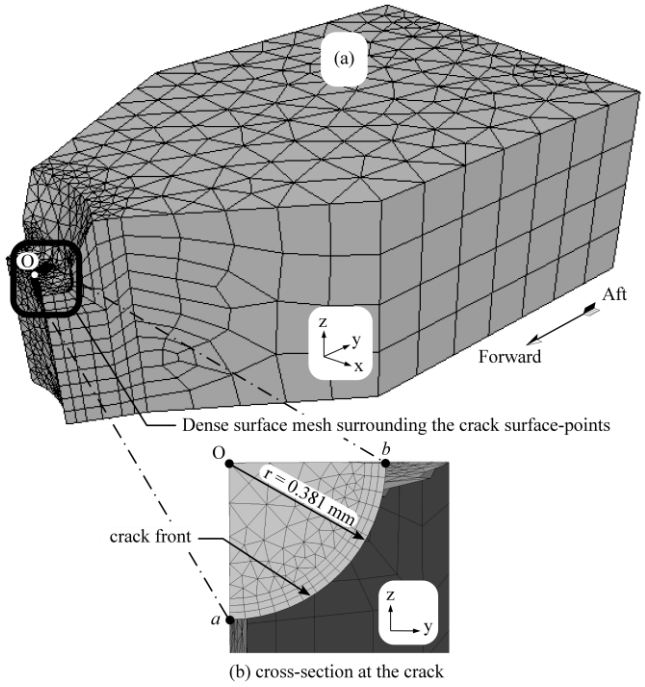

Fig. 12. Portion of analysis database, Σ_o, at initial step showing FE model of one side of bolt hole: (a) portion of subregion; and (b) one of the crack fronts. The point labeled O is the crack origin. The points labeled a and b are the crack front surface points.

fatigue specimen at hole 16 (top) and the crack growth steps of the Level II simulation (bottom). This allows qualitative visual validation. Generally, the simulated crack fronts compare well with the actual fracture surfaces, especially during the early, part of MSC growth. Thereafter, the observed crack front has more curvature, but comparison of what appear to be fatigue striations with the last 5 or so predicted shapes is not valid. These are not fatigue striations, but rather are pop-in markings, each associated with a few of the final spectrum cycles. Nevertheless, this comparison highlights some as yet unresolved issues in simulating fully 3D, arbitrary fatigue crack growth. Among these are: The K-range is computed assuming plane strain conditions at all locations along the crack front. This

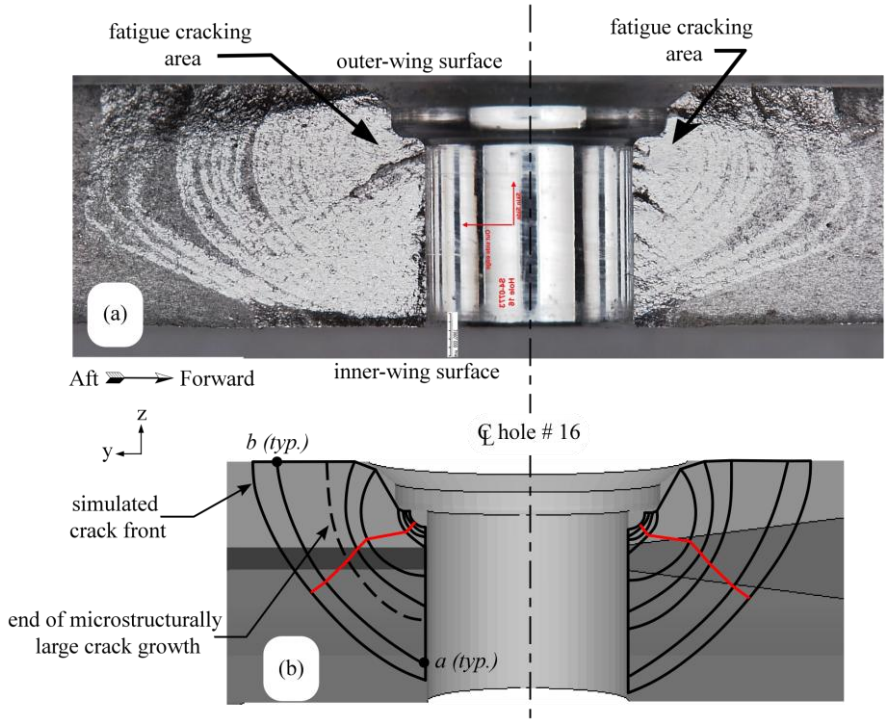

Fig. 13. Image of fracture surface at the aft side of bolt hole 16 (top) compared with the simulated fracture surface (bottom). Dotted, simulated crack front marks end of microstructurally large fatigue crack growth region, at n^{MLC} = 4070 cycles.

over-predicts the K-range at the plane stress, surface points on the crack front. Next, the algorithm to advance the crack front for each increment uses only the ratio of the SIFs and cannot account for varying fatigue resistance with material direction: in general, no point along the crack front is always moving in a constant material direction. Finally, the specimen was machined from a thick plate. Clearly, the thickening-pad on the stiffener-side (inner-wing surface) of the plate is deeper into the original plate than the outer-wing surface. This inevitably results in asymmetry in the material toughness, producing faster growth rates towards the outer-wing surface. Overall, it is inconclusive how these effects impact the Level II prediction of n^{MLC}.

The Level II life prediction is the result of cycle-by-cycle integration of the SIF histories conducted at three crack front points. The minimum life prediction is taken to be the high fidelity estimate of number of cycles consumed by microstructurally large crack growth, n^{MLC}. The life prediction was governed by the point which had the minimum number of cycles of 4,070. The Level I conservative estimate of n^{MLC} was only 147 cycles. With the update from Level II, the mean life prediction at the hot-spot, for spectrum loading with initial flaws from the particle filter, shifts from 29,058 cycles to 32,981 cycles of spectrum load. Applying the update at only one hot-spot has no visible affect on the total reliability of the structure. This is the expected result considering the summation in equation *.8 is over all surface nodes.

From the experiments conducted at NGC, the component failed after 53,485 cycles of fatigue loading. The minimum average Level I fatigue life prediction was 29,058, or, conservatively as desired, 46% less than the test. Including the update from the Level II simulation, that average life

prediction changed to 32,981, or 38% less than the test. However, there is no way to guarantee that the current hot-spot remains the location of minimum average life prediction without performing updates at all damage origins having Level I life predictions less than, or equal to, 32,981 cycles. Also, it is of interest to note that the predicted 4,070 cycles of microstructurally large crack growth are approximately 8% of the observed total fatigue life. This estimate agrees well with the literature that suggests microstructural growth processes can consume most of total fatigue life (Suresh 1998; Fan et al. 2001). Finally, the predicted probability of failure at 53,485 cycles is not affected by Level II updating of only one hot-spot.

6 DDSIM LEVEL III: HIGH-FIDELITY, MICROSTRUCTURALLY SMALL CRACK GROWTH SIMULATION

DDSim Level III is the third tier in the hierarchical fatigue life simulation. Level III directly couples FE models of the material microstructure with FE models of the structural length-scale. The microstructural models can include as much detail about phase, morphology, and texture as necessary to capture crack incubation and nucleation processes. Hence, the hot-spots selected from the Level I simulation are used as the focal points of the microstructural models. Much of the work supporting Level III is ongoing, as described in other chapters of this book. Nevertheless, the discussion here will include a vision for the final product which will result in a high-fidelity fatigue life prediction by accurately computing the number of cycles consumed by microstructurally small cracking processes.

The processes to be included are crack incubation, nucleation, and microstructurally small crack propagation.

The work presented here is intended to provide the foundation for further advancement of the DDSim methodology. Continued work is being done in the following arenas:

- development of FE models that are accurate statistical realizations of the microstructure of many important aerospace alloys, such as those discussed in other chapters of this book;
- development of models for the mechanics of microstructurally small crack propagation, and the damage processes discussed in other chapters;
- development of numerical methods to couple length scales; and
- development of statistical methods to maximize the efficiency of the DDSim methodology.

Many multiscale simulation approaches in the literature allow unilateral data flow either downward from the structural length scale, or upward from the microstructural length scale, by way of micromechanically informed constitutive modifications. Often, it is assumed that the local fields in the structural length scale model have negligible gradient over the relatively short dimensions of the microstructural model (Fish and Shek 2000; Fish and Belsky 1997). DDSim Level III is designed to allow two-way data flow. The FE models of the two length scales are either directly coupled with multipoint constraints, or with a modified multigrid approach that does not require homogenization (Bozek 2007; Datta et al. 2004). The microstructural damage is allowed to accumulate *in situ*, as it would in service, and the response is directly palpable by the structural scale model as envisioned within the evolution of the digital HyperFortress. That is, the fields resulting from the boundary conditions applied to the structural

model follow their preferred paths -- trickling down to the crystal lattice length scale -- and the material's response is propagated back upward.

6.1 Generation of a Microstructural Model

The microstructural model should be statistically realistic. Such a representation can begin with a grain morphology created by a simulated annealing process (Brahme et al. 2006; Saylor et al. 2004). This process itself begins by creating a Voronoi tessellation. Subsequently, the volume is densely packed with ellipsoids whose dimensions are generated from the observed statistics of grain dimensions. The grain geometry is created by grouping Voronoi cells whose centroids are contained within a common ellipsoid. After the geometry is generated, meshing is automatically completed using the same advancing front algorithm as in Level II. Both representations can include cracked second-phase particles, as described by Bozek et al. (2008) and Veilleux (2007). Figure 14(a) shows the geometry of a 128 grain polycrystal which includes 28 second-phase surface particles and 14(b) shows the surface mesh. The volume mesh of the polycrystal model shown in the figure consists of over 3.2M quadratic tetrahedra with over 13M degrees-of-freedom.

Finally, the mechanics of the crystallographic response are approximated with a crystal plasticity model (Matous and Maniatty 2004). This model includes the anisotropic elasto-plastic behavior of a grain, and includes parameters that describe the lattice orientation of the grain. The polycrystal model then accounts for texture by assigning orientations to grains based on observed statistics.

6.2 Level III Input and Operations

Figure 15 is the flowchart for the Level III simulation using the multipoint constraint approach. The input to Level III comes from Levels I and II, and includes the complete FE model of the structural length-scale. The geometry model of this scale is modified to accommodate the aforementioned polycrystal models. The polycrystal model is generated, the multipoint constraint equations are written, or the multigrid procedure is executed, and the multiscale model is analyzed. Following the analysis, the conditional probability of failure is computed and the loop is repeated as necessary. The following discussion elaborates on the process.

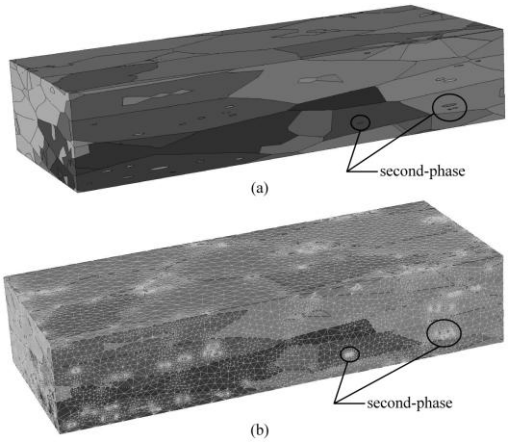

Fig. 14. A digital replication of a statistically accurate128 grain polycrystal of 7075-T651 which includes 28 second-phase particles: (a) the geometry; and (b) the surface mesh.

The input to Level III includes the structural length-scale FE model that was used to make the Level I predictions. The other essential inputs to Level III are the current hot-spot location, and the conditional reliability at that hot-spot. The former is required so that the structural model can be modified. The latter is required because it is conceivable that a Bayesian analysis could be developed whereby the Level I reliability prediction is

used as the prior distribution and is improved by only a few multiscale analyses.

Interactive tools have been created to modify automatically the geometry and mesh of the structural length-scale model. The first tool allows entry of the coordinate position of the centroid of the polycrystal model, information obtained from Level I. The next tool defines the region to be removed from the structural scale model. This tool automates this process and allows the user to control the mesh density on the new surfaces created during the process. Figure 16(a) shows the region definition and mesh density control panel. The mesh density control panel allows the user to control the number of elements along the edges of the

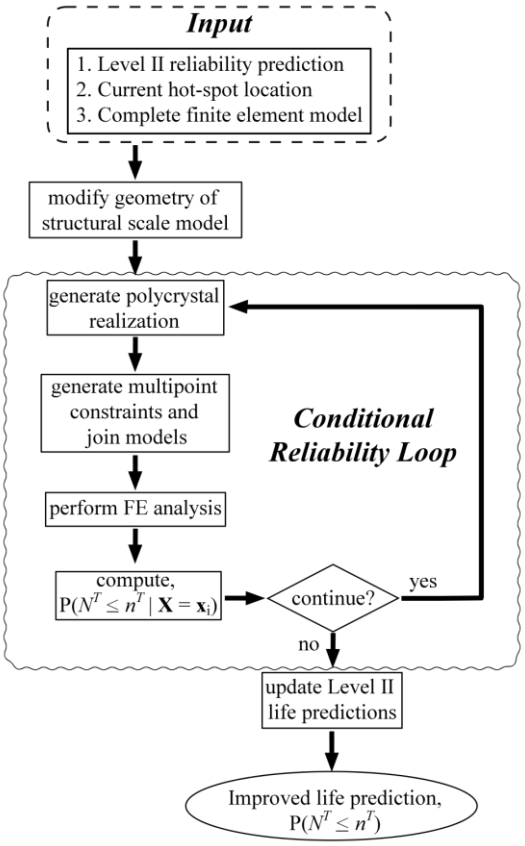

Fig. 15. DDSim Level III flowchart for the multipoint constraint approach..

void. Subsequently, the region can be rotated or translated, as shown in Figure 16(b), to allow the microstructural model to be aligned with the rolling, transverse and normal direction of the structure.

Figure 17 shows the renovated example model. The void to accommodate the polycrystal is circled in black. The automatically remeshed region, between the undisturbed structured mesh and the inserted polycrystal FE model, is obviously distinguishable.

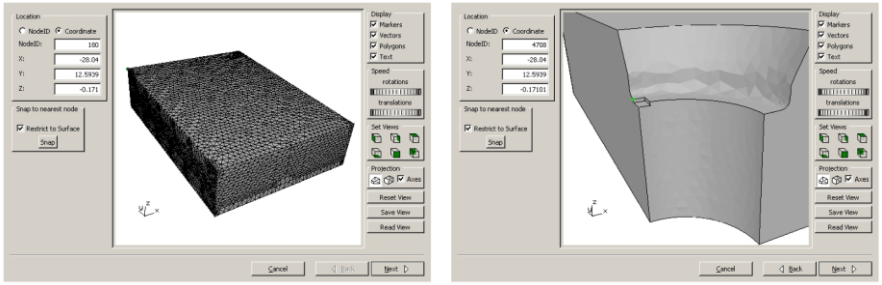

(a) (b)

Fig. 16. (a) The microstructure region definition and mesh control panel. (b) The region rotation and translation panel. Size and location of microstructural model shown.

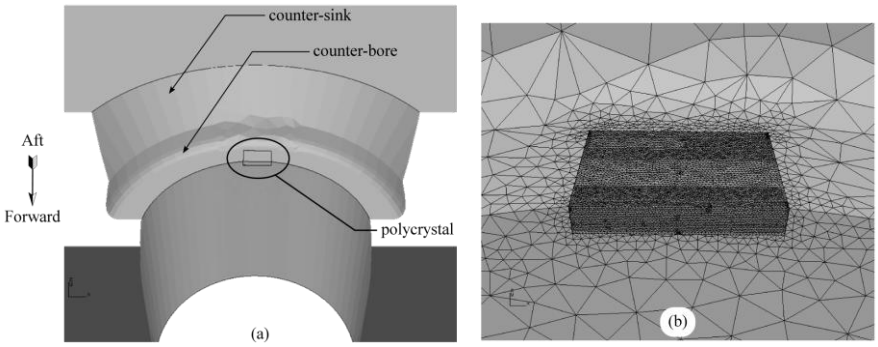

Fig 17. The renovated example (a) with the structure-scale mesh locally modified, and a polycrystal FE model inserted (b).

The conditional reliability loop is where the high fidelity prediction of conditional reliability for the given hot-spot is computed. The necessary steps for the multipoint constraint option are to:

- Generate the polycrystal realization;
- Generate the multipoint constraints and merge the models;
- Perform the FE analysis; and
- Compute the conditional reliability.

After the multiscale analysis, the conditional reliability is computed. The conditional reliability loop is repeated until the required fidelity at the

current hot-spot is achieved. After achieving adequate fidelity in the conditional reliability, the conditional reliability loop is exited and the total structural reliability is updated. With the total reliability updated at the current hot-spot, the simulation continues at the next hot-spot as shown in Figure 15. The details regarding the requisite number of iterations through the conditional reliability loop are beyond the scope of this chapter and are an open topic of research. However, if computing resources were not a limitation, the conditional reliability loop of Level III could be used in a Monte Carlo simulation with a large number of microstructural realizations.

6.3 Application of DDSim Level III to Example Problem

As noted earlier in this section, the rules of behavior for all the MSC processes are still being discovered and encoded, as evidenced by other chapters in this book. Therefore, a Level III update to N^{MSC} is not yet possible. However, it is possible to show how a microstructural model can be analyzed within the DDSim framework. The one-way example shown here is the two-phase polycrystal shown in Figure 14, under a single cycle of uniaxial straining. A result is depicted in Figure 18(a) which clearly shows the highly heterogeneous RD stress distribution resulting from crystal-plastic deformation operating on statistically accurate texture. Figure 18(b) shows

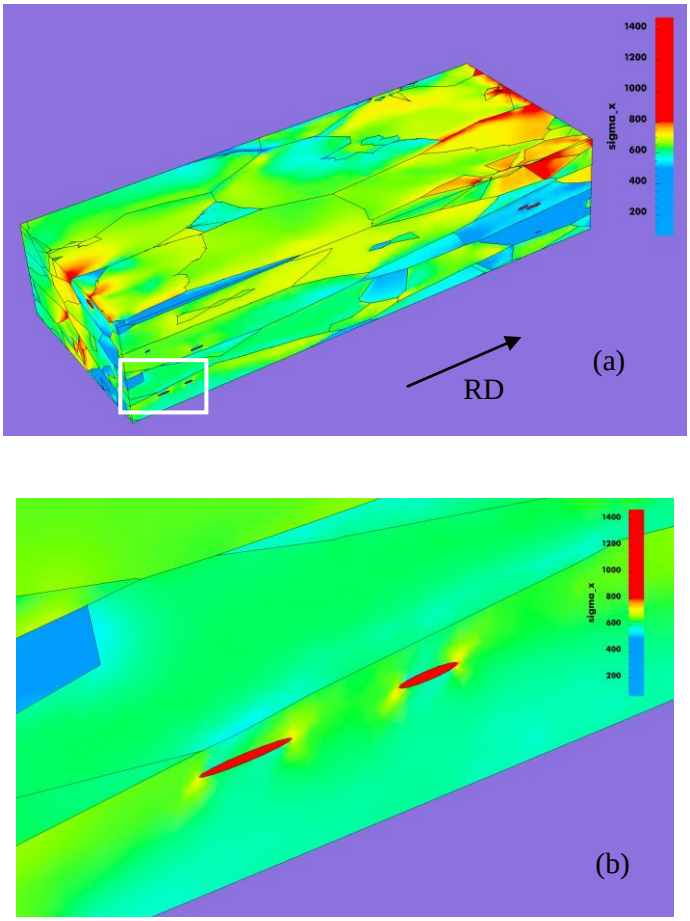

Fig 18. (a) Contours of RD normal stress (MPa) on microstructural model under a 1% RD applied strain. Boxed detail shown in (b) concentration around stiffer particles, note changed stress scale.

local fields around, and stress concentrations in, some of the stiffer surface particles, here idealized as semi-ellipsoids. This state would be the starting point for simulation of incubation in this alloy: particle cracking. This would be followed by the nucleation stage, during which some of the cracked particles spawn intragranular cracks, the MSC propagation stage leading to intergranular cracking and coalescence, and, ultimately, the MLC stage leading to component failure. The physics, mechanics, and

statistics of all these stages need to be discovered or tested for validity in this new era of combined physical and computational simulation.

This single elasto-crystal plastic analysis required about 64 hours to execute on a 240 (single core, 3.6 GHz) processor cluster, with a parallel FE code developed by the Cornell Fracture Group (FRANC3D/NG 2008). The code uses PETSc (Balay et al. 2006) for parallel equation solving, and an in-house FE library, FemLib, for element and constitutive formulations. Again, the need for exascale computing power for reliable prognosis for "digital aircraft" is evident.

7 CONCLUSIONS

Highly detailed digital instantiations of future air vehicles will co-exist with their tangible counterparts. With such "digital aircraft" as both database and virtual sensor, computational simulations of material degradation and structural performance will be done during design, development, testing, and service. This chapter described a humble prototype of a system within which multi-scale simulations of fatigue cracking could be coherently performed.

DDSim's hierarchical design allows reduced-order, fast searches for likely trouble spots across the many FE models which will exist for the primary structural components of airframe and engine. It predicts a conservative reliability estimate for each, and then offers opportunities to improve the fidelity of the reliability prediction. Rigorous component-scale FE simulations can then be performed to improve the reliability of the MLC portion of total life. In addition, material-scale simulations can be performed at these trouble spots, involving all the developments in understanding of nano- and microstructural damage processes described in

the other chapters of this book, to improve reliability of the MSC portion of life.

Much work remains to be done to reach the vision offered in the prologue to this chapter. To "*...uncover and quantify material and structural limit states with reliability predictions...*" the rules of physics and mechanics, governing all aspects of fully 3D MSC processes, still need to be discovered. The stochastics of these processes will then have rational explanation. These rules must then be properly encoded, within software not yet invented, that can executed efficiently, on computers not yet built, *so we can use our"... most advantageous tool—nearly infinite computing power.* "

8 ACKNOWLEDGEMENTS

The authors gratefully acknowledge partial sponsorship for the research reported here by the Defense Advanced Research Projects Agency under contract HR0011-04-C-0003, Dr. Leo Christodoulou, Program Manager, and by NASA through the Constellation University Institutes Program, grant number NCC3-994. The authors also thank Drs. Wash Wawrzynek and Bruce Carter for their development of FRANC3D/NG.

9 REFERENCES

AFGROW Users' Guide and Technical Manual. (2008) Technical Report AFRL-VA-WP-TR-2008-XXXX, Air Force Research Laboratory, WPAFB, OH

ANSYS, Release 10.0, (2006) ANSYS, Inc. Canonsburg, PA

Balay S, Buschelman K, Eijkhout V, Gropp W, Kaushik D, Knepley M (2006) PETSc Users Manual. Argonne National Laboratory report anl-95/11-rev. 2.3.2 edn

Banks-Sills L, Hershkovitz I, Wawrzynek PA, Eliasi R, Ingraffea AR (2005) Methods for calculating stress intensity factors in anisotropic materials: Part I – z=0 is a symmetric plane. Eng Fract Mech, 72:2328– 2358

Banks-Sills L, Wawrzynek PA, Carter BJ, Ingraffea AR, Hershkovitz I (2007) Methods for calculating stress intensity factors in anisotropic materials: Part II – arbitrary geometry. Eng Fract Mech 74:1293– 1307

Bozek JE (2007) A 2D Multiscale Procedure for Fatigue Crack Nucleation. M.S. Thesis, Cornell University

Bozek JB, Hochhalter JD, Veilleux MG, Liu M, Heber G, Sintay SD, Rollett AD, Littlewood DJ, Maniatty AM, Weiland H, Christ Jr. RJ, Payne J, Welsh G, Harlow DG, Wawrzynek PA, Ingraffea AR (2008) A geometric approach to modeling microstructurally small fatigue crack formation, part I: probabilistic simulation of constituent particle cracking in AA 7075-T651. Mod Sim Mat Sci Eng 16: article number 065007

Brahme A, Alvi MH, Saylor D, Fridy J, Rollett AD (2006) 3D reconstruction of microstructure in a commercial purity aluminum. Scripta Mater 55:75–80

Carter BJ, Wawrzynek PA, Ingraffea AR (2000) Automated 3-D crack growth simulation. Int J Num Meth Eng 47:229–253

Datta DK, Picu RC, Shepard MS (2004) Composite Grid Atomistic Continuum Method: An Adaptive Approach to Bridge Continuum with Atomistic Analysis. Int. J. Multiscale Comp. Eng., 2(3): 401-419

Emery J (2007) Hierarchical, Probabilistic, Damage and Durability Simulation Methodology. Ph.D. thesis, Cornell University

Emery J, Hochhalter J, Wawrzynek PA, Ingraffea A R (2008) DDSim: A hierarchical, probabilistic, multiscale damage and durability simulation methodology – Part I: methodology and Level I. Eng Fract Mech, in press.

Fan J, McDowell DL, Horstemeyer MF, Gall K (2001) Computational micromechanics analysis of cyclic crack-tip behavior for microstructurally small cracks in dual-phase al-si alloys. Eng. Fract. Mech. 68:1687-706

Fish J, Shek KL (2000) Multiscale Analysis of Large Scale Nonlinear Structures and Materials. Int J Comp Civil Struct Eng 1(1): 79-90

Fish J, Belsky V (1997) Generalized Aggregation Multilevel Solver. Int J Num Meth Eng, 40(23): 4341-4361

Forman RG, Mettu SR (1992) Behavior of surface and corner cracks subjected to tensile and bending loads in Ti-6Al-4V alloy. In: Fracture Mechanics: Twenty second Symposium, ASTM STP-1131, American Society for Testing and Materials, Philadelphia, pp 519–546

FRANC3D/NG, Three-dimensional fracture analysis code. (2008) http://www.cfg.cornell.edu/software/software.htm. The Cornell Fracture Group. Cornell University, Ithaca, NY.

Ingraffea AR (2008) Computational Fracture Mechanics. In: Stein E, de Borst R, Hughes T (eds) Encyclopedia of Computational Mechanics, 2nd edn, John Wiley and Sons, New York, Volume 2, Chapter 11.

NASGRO fatigue crack growth analysis software, version 5.2 (2008). Southwest Research Institute and National Aeronautics and Space Administration.

Matous K, Maniatty A (2004) Finite element formulation for modelling large deformations in elasto-viscoplastic polycrystals Int J Num Meth Eng 60:2313-33

Neto JCB, Wawrzynek PA, Carvalho MTM, Martha LF, Ingraffea AR (2001) An algorithm for three-dimensional mesh generation for arbitrary regions with cracks. Eng Comp 17:75–91

Neto JCB, Miranda A, Martha L, Wawrzynek PA, Ingraffea AR (2008) Surface mesh regeneration considering curvatures, Eng Comp, in press

Papazian JM, Anagnostou EL, Engel SJ, Fridline DR, Hoitsma DH, Madsen JS, Silberstein RP, Whiteside JB (2007) Structural Integrity Prognosis. In: Lazzeri L, Salvetti A (eds) Proceedings 24th Symposium of the International Committee on Aeronautical Fatigue. pp. 109-125

Papazian JM, Anagnostou EL, Engel SJ, Fridline DR, Hoitsma DH, Madsen JS, Nardiello J, Silberstein RP, Welsh G, Whiteside JB (2007) SIPS, A Structural Integrity Prognosis System. In: Proceedings 2007 IEEE Aerospace Conference, Big Sky MT, paper no. 11.0901 (T11/ Z11_0901)

Saylor DM, Fridy J, El-Dasher BS, Jung KY, Rollett AD (2004) Statistically representative three-dimensional microstructures based on orthogonal observation sections. Metal Mat Trans 25A(7):1969–1979

Suresh S (1998) Fatigue of Materials. Cambridge University Press, Cambridge; New York

Veilleux MG (2007) Finite element model generation of statistically accurate 7075-T651 aluminum alloy microstructures. M.S. thesis, Cornell University

List of Symbols

$\boldsymbol{A}$	random vector, p-dimensional array describing flaw geometry
a^{MLC}	the characteristic length of a crack when it can be considered microstructurally large
$\boldsymbol{C}$	crack growth function
CDF	cumulative distribution function
$\boldsymbol{E}$	random vector, s-dimensional array describing material resistance to crack growth
N^T	a random variable, the total fatigue life of a structure, integer, cycles
N^{MLC}	a random variable, the number of cycles consumed by microstructurally large crack growth processes
N^{MSC}	a random variable, the number of cycles consumed by microstructurally small crack growth processes
n^{MLC}	a realization of N^{MLC}
n^{MSC}	a realization of N^{MSC}
n^T	a realization of N^T
n^T_{cr}	a critical realization of N^T
$\boldsymbol{D}$	discretization process
$\boldsymbol{F}$	fracture mechanics process
FE	finite element
FLOPS	floating-point operations per second
$\boldsymbol{K_i}$	crack driving force database
MLC	microstructurally large crack
MSC	microstructurally small crack
P_f	probability of failure

$\boldsymbol{Q_i}$.	equilibrium database
R	reliability
R	load ratio
RMS	root mean square
RD	rolling direction
$\boldsymbol{R_i}$	representational database
$\boldsymbol{S}$	solution procedure
TD	transverse direction
ND	normal direction
$\boldsymbol{U}$	update function
$\boldsymbol{X}$	random vector, dominant flaw location
$\boldsymbol{\Sigma_i}$	stress analysis database